TITLE:

In vivo KRAS G12D/V Degradation Mediated by CANDDY Using a Modified Proteasome Inhibitor

AUTHORS/AFFILIATIONS:

Satoshi Imanishi[1,#], Lijuan Huang[1,#], Shoko Itakura[2], Masamichi Ishizaka[1], Megumi Tsukamoto[1], Megumi Saito[1], Yoichi Iwasaki[1], Tomohiro Yamaguchi[1], and Etsuko Miyamoto-Sato[1,2*]

[1] Laboratory of Miyamoto-Sato Molecular Medical Sciences, Research Institute for Science & Technology, Tokyo University of Science, 2641 Yamazaki, Noda, Chiba 278-0022, Japan

[2]Graduate School of Biological Sciences, Tokyo University of Science, 2641 Yamazaki, Noda, Chiba 278-0022, Japan

[#]These authors contributed equally to this work.

[*] Correspondence: nekoneko@rs.tus.ac.jp

Summary paragraph

"Undruggable" proteins, such as RAS proteins, remain problematic despite efforts to discover inhibitors against them. KRAS mutants are prevalent in human cancers. Although KRAS G12C inhibitors have been developed recently, there are no effective inhibitors for KRAS G12D/V. Here, we described the development of a novel chemical knockdown strategy, termed CANDDY (Chemical knockdown with Affinity aNd Degradation DYnamics). This strategy, which is not an inhibition strategy, involves a CANDDY tag modified from a proteasome inhibitor. The tag induces direct proteasomal degradation. We constructed TUS-007 as a multispecific small molecule tethered from a KRAS interactor and CANDDY tag to target KRAS G12D/V. TUS-007 successfully suppressed tumors due to the degradation of KRAS G12D/V. We confirmed that the CANDDY tag-induced degradation was independent of target ubiquitination. The CANDDY technology could represent a simple and practical way to degrade currently "undruggable" proteins.

The majority (75%) of disease-causing proteins are "undruggable" (i.e., difficult to inhibit with small molecules). This difficulty reflects in the presence of smooth surfaces and lack of deep pockets, including proteins associated with cancer drivers and many interfaces for protein-protein interaction (PPI) (1, 2, 3). RAS family members (e.g., KRAS, HRAS, and NRAS) are most challenging to inhibit by small molecules (1, 4, 5, 6, 7). Mutations of KRAS, especially G12C, G12D, and G12V, are frequent in human cancers (7). The RAS protein activities depend on nucleotide loading in their GTP-binding pockets. The inhibition of this pocket has been attempted for nearly 40 years. However, progress has been hindered by the exceptionally high affinity between GTP and RAS proteins (1, 4, 8). While clinically effective inhibitor candidates targeting KRAS G12C have been developed recently (6, 9), there is still no effective inhibitor for KRAS G12D/V. These are important targets found in 95% of pancreatic cancers and 64% of colon cancers (7, 8). Inhibitors of the PPI between RAS and Son of Sevenless 1 (SOS1) (RAS-SOS inhibitor) have been investigated. Inhibitors that directly bind to RAS are not effective owing to their low affinity (5). Thus, the current inhibition technologies are not enough to be effective for undruggable proteins.

Pharmaceutical research on undruggable proteins, such as RAS, focuses on novel modalities instead of inhibition (10, 11, 12). Protein destabilization technologies, using matchmakers between the target and E3 ligase for target ubiquitination, are expected to be effective against undruggable proteins (13, 14, 15, 16, 17). However, matchmaker design has been hampered by the dependency on target ubiquitination (16). It is difficult to select a suitable E3 ligase for a target of interest because of limited knowledge about the mechanism underlying substrate recognition by E3 ligases. Even if the target has an established corresponding E3 ligase, there may be no available ligand for the E3 ligase. Moreover, target ubiquitination may not always induce proteolysis, as in the case of RAS, in which ubiquitination also regulates protein localization and activation (18). Despite such difficulties, an effective inhibitor (9) was used recently for a proteolysis inducer of KRAS G12C (19). However, no proteolysis inducer for KRAS G12D/V has been reported. Current protein destabilization technologies that depend on ubiquitination have limited efficacy for undruggable targets (14). Therefore, to modulate diverse undruggable targets, the difficulties in matchmaking should be eliminated (13).

Here, we report successful KRAS G12D/V degradation, mediated by a novel tool named CANDDY (Chemical knockdown with Affinity aNd Degradation DYnamics). This innovative approach induces direct proteasomal degradation (i.e., chemical knockdown) of the target using a CANDDY tag derived from a proteasome inhibitor that lacks the site for inhibitory activity (inhibitor site). In principle, chemical knockdown occurs without ubiquitination, so it can bypass the difficulties of designing a matchmaker in current protein destabilization techniques (13). To evaluate the utility of CANDDY, we developed a CANDDY molecule called TUS-007 for KRAS G12D/V and demonstrated its application in KRAS G12D/V chemical knockdown in cell-free, *in vitro*, and *in vivo* assays and *in vivo* tumor suppression.

A CANDDY molecule for targeting KRAS G12D/V proteins

CANDDY molecules are bispecific molecules constructed from two modules; a target interactor, which enables specific binding to the target, and a CANDDY tag, which induces proteasomal degradation (Fig. 1a). The CANDDY tag is essential in CANDDY technology and is a derivative lacking the inhibitor site of MLN2238 (MLN)

79 (20), a clinical proteasome inhibitor (Fig. 1b and Additional Information). To design
80 TUS-007, we employed a RAS-SOS inhibitor (5) (shown in Fig. 1c) which directly
81 binds to KRAS G12D, KRAS G12V, and wild-types of KRAS and HRAS as the target
82 interactor module. Since the binding to wild-type NRAS have not been reported, it was
83 expected to avoid the severe toxicity observed in a pan-RAS inhibitor (21). RAS-SOS
84 inhibitor was conjugated to the CANDDY tag using an NH_2 linker (Fig. 1c and
85 Additional Information).
86 To compare the target binding of TUS-007 with that of the RAS-SOS
87 inhibitor, we performed a thermal shift assay. Unexpectedly, KRAS G12D/V proteins
88 incubated with TUS-007 were more resistant against heat treatment than those
89 incubated with RAS-SOS inhibitor (Fig. 1d). Alternatively, in a fluorescence-based
90 thermal shift assay, the T_m value of KRAS G12D incubated with TUS-007 was higher
91 than that of KRAS G12D incubated with RAS-SOS inhibitor (Supplementary Fig. 1).
92 These results suggest the higher affinity of TUS-007 to KRAS compared to RAS-SOS
93 inhibitor. In addition, we confirmed that TUS-007 had no inhibitory activity against the
94 catalytic β-subunits of proteasome (Supplementary Fig. 2). This demonstrated that the

CANDDY tag, modified from a proteasome inhibitor, hardly inhibit proteasome activity.

A CANDDY molecule degraded KRAS G12D/V proteins in cell-free assay

We attempted a chemical knockdown of KRAS G12D in the presence of 26S proteasomes and in the absence of E3 ligase in a cell-free assay. Successful degradation was performed (Fig. 1e) with 50% degradation concentration (DC50) at 4 μM (Supplementary Fig. 3a). The chemical knockdown mediated by TUS-007 was counteracted by the presence of MLN (Supplementary Fig. 3b). Additionally, RAS-SOS-NH_2 as a degradation-incompetent control failed to induce the chemical knockdown (Supplementary Fig. 3b), demonstrating CANDDY tag is essential to induce the chemical knockdown. Although RAS-SOS inhibitor showed 80% inhibition of RAS-SOS PPI at 1 mM (5), DC80 of TUS-007 for KRAS G12D was estimated as 16 μM (Supplementary Fig. 3a). It implied that the conjugation with CANDDY tag drastically improved the usefulness of RAS-SOS inhibitor. We also confirmed chemical knockdown of KRAS G12V by TUS-007 in a cell free assay (Supplementary Fig. 3c).

Thus, the chemical knockdown of KRAS G12D/V by TUS-007 depended only on proteasomes and not on ubiquitination. Importantly, the conjugation of CANDDY tag enabled the direct proteasomal induction and the simple cell free assay for chemical knockdown could be applied, because of the lack of ubiquitination process.

TUS-007 induced targets-selective chemical knockdown *in vitro*

Using an *in vitro* assay, we then evaluated the chemical knockdown and investigated the selectivity of TUS-007. We utilized RAS-less mouse embryonic fibroblasts (MEFs) expressing human KRAS G12D, G12V, or G12C. These MEFs do not proliferate in the absence of RAS (22). Immunoblotting analysis revealed that TUS-007 induced the chemical knockdown of KRAS G12D/V, but not G12C, in RAS-less MEFs (Fig. 1f). TUS-007 reduced the viability of RAS-less MEFs expressing KRAS G12D/V but did not affect the viability of the cells expressing KRAS G12C (Fig. 1g), confirming the selectivity of TUS-007 for KRAS G12D/V. Moreover, the results from RAS-less MEFs expressing KRAS G12C showed that TUS-007 did not cause non-specific cytotoxic effects even for high concentrations such as 100 μM (Fig. 1f & g).

Additionally, we assessed the selectivity of TUS-007 for the human RAS family, including wild-type KRAS, HRAS, and NRAS. TUS-007 did not affect the NRAS protein levels or the viability of RAS-less MEFs expressing NRAS but attenuated KRAS and HRAS levels and reduced the viability of RAS-less MEFs expressing KRAS and HRAS (Supplementary Fig. 4a and b). This result is consistent with the previously reported data on the selectivity of the RAS-SOS inhibitor (5). Therefore, considering that TUS-007 is not a pan-RAS degrader, it is expected not to induce intolerable toxicity, as has been previously observed with a pan-RAS inhibitor *in vivo* (21). Furthermore, the viability of RAS-less MEFs expressing KRAS G12C or NRAS maintained even at 100 μM TUS-007. These results suggested that TUS-007 did not have remarkable off-target effect resulting in toxicity in cell even at high concentrations.

TUS-007 exerted anti-tumor activity against KRAS G12V-driven colon cancer

Approximately 64% of human colon cancers reportedly express KRAS mutants. KRAS G12V is found in nearly half of the patients and is correlated with poor

143 prognosis (8). Therefore, we investigated whether TUS-007 can suppress the growth of
144 human KRAS G12V-driven colon cancer cells. We conducted an experiment with the
145 SW620-Luc KRAS G12V homozygous human colon cancer cell line (23). TUS-007
146 induced chemical knockdown of KRAS (Fig. 2a), accompanied by an increase in the
147 annexin V-positive fraction in SW620-Luc cells (Fig. 2b). However, RAS-SOS-NH_2 (a
148 synthetic intermediate without CANDDY tag, Fig. 1c) and cetuximab did not induce
149 apoptosis (Fig. 2b and Supplementary Fig. 5). In contrast, treatment with TUS-007 did
150 not result in significant changes in the annexin V-positive fraction in HT29-Luc RAS-
151 independent colon cancer cells (Fig. 2c and Supplementary Fig. 6). Alternatively, the
152 apoptosis induction in SW620-Luc cells was confirmed by caspase 3/7 activation (Fig.
153 2d). Importantly, TUS-007 induced the apoptosis in SW620-Luc cells at the same
154 concentration at which the chemical knockdown of KRAS was significant (Fig. 2a and
155 b). These findings indicated that TUS-007 selectively induces apoptosis in SW620-Luc
156 cells by chemical knockdown of KRAS G12V *in vitro*. Additionally, the results in
157 HT29-luc cells also indicated no remarkable off-target effect resulting in toxicity even
158 at high concentrations.

159 Next, to assess the effectiveness of TUS-007 *in vivo*, we transplanted SW620-
160 Luc cells subcutaneously in immunodeficient mice. TUS-007 or cetuximab was
161 administered to the xenograft mice by intraperitoneal (i.p.) injection. TUS-007
162 significantly attenuated tumor progression (Fig. 2e; Supplementary Fig. 7a and b) and
163 induced KRAS G12V chemical knockdown in tumors (Fig. 2f). The body weights of
164 the mice were not affected by TUS-007 treatment (Supplementary Fig. 7c). These
165 results suggested that TUS-007 is effective *in vivo* against KRAS G12V-driven tumors.
166
167 **TUS-007 exerted anti-tumor activity against KRAS G12D-driven pancreatic**
168 **cancer**
169 Approximately 95% of pancreatic cancers harbor KRAS mutations, and the
170 G12D mutation is particularly prevalent and strongly correlated with poor prognosis (8).
171 Therefore, we examined the effects of TUS-007 in human pancreatic cancer cell lines.
172 As expected, TUS-007 degraded the KRAS protein (Fig. 3a) and induced apoptosis
173 (Fig. 3b) in SW1990 KRAS G12D-driven pancreatic cancer cells (24). In addition,
174 apoptosis was induced with caspase 3/7 activation in SW1990 cells (Fig. 3c), which was

175 counteracted by the proteasome inhibitor MLN but not by the NAE E3 ligase inhibitor
176 (NAEi) (Fig. 3d). Furethermore, the apoptosis induction in SW1990 cells was detected
177 around concentrations of chemical knockdown of KRAS (Fig. 3a and b). Therefore, it
178 suggested that TUS-007 induced apoptosis owing to target degradation independent of
179 ubiquitination.

180 In mice with SW1990 cells implanted subcutaneously, the oral (per os; p.o.)
181 administration of TUS-007 significantly suppressed the tumor growth (Fig. 3e and
182 Supplementary Fig. 8a) and reduced tumor weight (Supplementary Fig. 8b). The i.p.
183 injection of TUS-007 also supressed subcutaneously implanted tumor growth in mice
184 (Supplementary Fig. 8c). Both p.o. (Fig. 3f) and i.p. (Supplementary Fig. 8d)
185 administrations showed no change in body weight. Here, we examined the chemical
186 knockdown of KRAS, HRAS and NRAS with TUS-007 in pancreas from the identical
187 mice used in Fig. 3e & f. In accordant with the results in RAS-less MEFs, TUS-007
188 induced the degradation of KRAS and HRAS but not NRAS (Supplementary Fig 10).
189 Thus, there was no sign of toxicity such as body weight losses in contrast to a pan-RAS
190 inhibitor (21).

Moreover, extracellular signal-regulate kinase (ERK) and AKT phosphorylation were decreased by both p.o. and i.p. administrations (Supplementary Fig. 9a & b), indicating that both RAS-mitogen-activation protein (RAS-MAP) and RAS- phosphoinositide 3-kinase (RAS-PI3K) signaling were inhibited. It is difficult for inhibitors to inhibit both RAS-MAP and RAS-PI3K signaling, even using a clinically effective KRAS G12C inhibitor (6). Thus, the chemical knockdown of KRAS by CANDDY might offer a clinical benefit. Taken together, these results indicated that TUS-007 exerted *in vivo* antitumor activity *via* the chemical knockdown of KRAS G12D/V and suppression of KRAS signaling.

Here, when an i.p dose of 80 mg/kg TUS-007 was administered to healthy mice, a concentration (45 ng/mg, equivalent to 53 μM) of TUS-007 was observed in the pancreas (Supplementary Table 1.). This TUS-007 concentration *in vivo* agreed with the concentration at which chemical knockdown and apoptotic indicators were observed in SW1990 cells *in vitro* (Fig. 3a, b and c). Therefore, these results suggest that there is no contradiction between our *in vivo* and *in vitro* results.

TUS-007 exerted anti-tumor activity even in orthotopic xenograft model mice

Finally, SW1990-Luc cells were transplanted directly into the pancreas of mice as an orthotopic xenograft model. The mice were subsequently treated p.o. with TUS-007. Remarkably, *in vivo* imaging revealed reductions in tumor growth (Fig. 4a and b; Supplementary Fig. 11a) and tumor weight (Supplementary Fig. 11b). Results from immunohistochemical analysis (Fig. 4c left panels and left bar graph) and immunoblotting (Supplementary Fig. 11c) confirmed the chemical knockdown of KRAS G12D in the tumor tissues of mice treated with TUS-007. Furthermore, higher concentrations of positive cells were observed in the terminal deoxynucleotidyl transferase dUTP nick-end labeling (TUNEL) assay in the tumor tissues of TUS-007-treated mice, implying the induction of apoptosis in the TUS-007-treated tumors (Fig. 4c right panels and right bar graph). The body weights of the orthotopic xenograft model mice were not affected by TUS-007 (Supplementary Fig. 11d). Overall, these results demonstrated that oral treatment with TUS-007 induces KRAS G12D chemical knockdown and suppresses pancreatic tumor growth without the sign of weight loss and significant toxicity in the orthotopic xenograft model.

223

224 **CANDDY applied to another undruggable target**

225 To evaluate the versatility of CANDDY approach, we designed a CANDDY
226 molecule targeting MDM2 (MDM2-CANDDY), a negative regulator of P53, using a
227 P53-MDM2 PPI inhibitor (25) as an interactor module of a CANDDY molecule
228 (Supplementary Fig. 12a and Additional Information). MDM2-CANDDY successfully
229 induced the chemical knockdown of MDM2 in HCT-116 human colon cancer cells
230 (Supplementary Fig. 12b). Although the reactivation of P53 by inhibition of MDM2 has
231 been expected as a novel therapeutic approach (26), P53-MDM2 PPI is still well-
232 recognized "undruggable" target. This result suggested the potential versatility of
233 CANDDY to target other undruggable proteins.

234

235 No effective drug to inhibit or degrade KRAS G12D/V has been reported yet.
236 TUS-007 successfully induced chemical knockdown of KRAS G12D/V, resulting in
237 tumor suppression *in vivo*. Generally, it has been difficult to find effective inhibitors for
238 undruggable targets. Nevertheless, just conjugating CANDDY tag to RAS-SOS

239 inhibitor produced TUS-007, an effective agent even for oral administrations *in vivo*.

240 Our results demonstrated that TUS-007 induced chemical knockdown of KRAS

241 G12D/V *via* a proteasomal process, which was independent of ubiquitination.

242 Importantly, we confirmed that chemical knockdown of KRAS induced

243 apoptosis (Fig. 2a and b; Fig. 3a and b). Also, the consistency between our *in vivo* and

244 *in vitro* results was confirmed by the pancreatic concentration of TUS-007, which

245 agreed with the effective concentratin *in vitro* (Fig. 3a, b and c; Supplementary Table1).

246 Additionally, a previous study showed that the moderate decrease of KRAS

247 protein inhibited tumor growth via more strong inhibition of downstream signal (12),

248 similarly as that in Supplementary Fig. 9a & b. In fact, the chemical knockdown of

249 KRAS by TUS-007 was moderate (Supplementary Fig. 11c) but suppressed the tumor

250 growth *in vivo* (Fig. 4a and b). The future study of TUS-007 may overcome the current

251 clinical challenge related to the treatment refractory nature of KRAS G12D/V-positive

252 neoplasms.

253 The CANDDY tag, which was modified from a proteasome inhibitor, can

254 eliminate the difficulties of matchmaking in current protein degradation (13),

considering that proteasomes, unlike E3 ligases, have no substrate selectivity. Moreover, CANDDY tag was also effective in degrading MDM2 (Supplementary Fig. 12). These results suggest that CANDDY technology could be applied to other undruggable targets without efficient inhibitors. Hence, CANDDY technology could provide a simple and practical approach to induce the chemical knockdown of currently undruggable targets.

References

1. Khan, I., Rhett, J. M. & O'Bryan, J. P. Therapeutic targeting of RAS: New Hope for drugging the "undruggable". *Biochim. Biophys. Acta Mol. Cell Res.* **1867**, 118570 (2020).

2. Fujimori, S., et al. Next-generation sequencing coupled with a cell-free display technology for high-throughput production of reliable interactome data. *Sci. Rep.* **2,** 691 (2012).

3. Scott, D. E., Bayly, A. R., Abell, C. & Skidmore, J. Small molecules, big targets: Drug discovery faces the protein-protein interaction challenge. *Nat. Rev. Drug Discov.* **15,** 533–550 (2016).

4. Stephen, A. G., Esposito, D., Bagni, R. K. & McCormick, F. Dragging Ras back in the ring. *Cancer Cell* **25,** 272–281 (2014).

5. Sun, Q., et al. Discovery of small molecules that bind to K-Ras and inhibit Sos-mediated activation. *Angew. Chem. Int. Ed.* **51,** 6140–6143 (2012).

6. Canon, J., et al. The clinical KRAS(G12C) inhibitor AMG 510 drives anti-tumour immunity. *Nature* **575,** 217–223 (2019).

7. Hobbs, G. A., Der, C. J. & Rossman, K. L. RAS isoforms and mutations in cancer at a glance. *J. Cell Sci.* **129,** 1287–1292 (2016).

8. Haigis, K. M. KRAS alleles: The devil is in the detail. *Trends Cancer* **3,** 686–697 (2017).

9. Sheridan, C. Grail of RAS cancer drugs within reach. *Nat. Biotechnol.* **38,** 6–8 (2020).

10. Shin, S. M., et al. Antibody targeting intracellular oncogenic Ras mutants exerts anti-tumour effects after systemic administration. *Nat. Commun.* **8,** 15090 (2017).

11. Yin, W. & Rogge, M. Targeting RNA: A transformative therapeutic strategy. *Clin. Transl. Sci.* **12,** 98–112 (2019).

12. Ross, S. J., et al. Targeting KRAS-dependent tumors with AZD4785, a high-affinity therapeutic antisense oligonucleotide inhibitor of KRAS. *Sci. Transl. Med.* **9,** pii: eaal5253. doi: 10.1126/scitranslmed.aal5253 (2017).

13. Deshaies, R. J. Multispecific drugs herald a new era of biopharmaceutical innovation. *Nature* **580,** 329–338 (2020).

14. Scudellari, M. Protein-slaying drugs could be the next blockbuster therapies. *Nature* **567,** 298–300 (2019).

15. Cromm, P. M. & Crews, C. M. Targeted protein degradation: From chemical biology to drug discovery. *Cell Chem. Biol.* **24,** 1181–1190 (2017).

16. Pettersson, M. & Crews, C. M. PROteolysis TArgeting Chimeras (PROTACs) - Past, present and future. *Drug Discov. Today Technol.* **31,** 15–27 (2019).

17. Churcher, I. Protac-induced protein degradation in drug discovery: Breaking the rules or just making new ones? *J. Med. Chem.* **61,** 444–452 (2018).

18. Dohlman, H. G. & Campbell, S. L. Regulation of large and small G proteins by ubiquitination. *J. Biol. Chem.* **294,** 18613–18623 (2019).

19. Bond, M. J., et al. Targeted degradation of oncogenic KRASG12C by VHL-recruiting PROTACs. *ACS Cent. Sci.* **6**, 1367–1375 (2020).

20. Kisselev, A. F., van der Linden, W. A. & Overkleeft, H. S. Proteasome inhibitors: An expanding army attacking a unique target. *Chem. Biol.* **19,** 99–115 (2012).

21. Welsch, M. E., et al. Multivalent small-molecule pan-RAS inhibitors. *Cell* **168,** 878–889.e29 (2017).

22. Drosten, M., et al. Genetic analysis of Ras signaling pathways in cell proliferation, migration and survival. *EMBO J*. **29,** 1091–1104 (2010).

23. Ahmed, D., et al. Epigenetic and genetic features of 24 colon cancer cell lines. *Oncogenesis* **2,** e71 (2013).

24. Jansen, J. M., et al. Inhibition of prenylated KRAS in a lipid environment. *PLOS ONE* **12,** e0174706 (2017).

25. Kumar, S. K., et al. Design, synthesis, and evaluation of novel boronic-Chalcone derivatives as antitumor agents. *J. Med. Chem*. **46**, 2813–2815 (2003).

26. Shangary, S. & Wang, S. Targeting the MDM2-p53 Interaction for Cancer Therapy. *Clin. Cancer. Res*. **14,** 5318–5324 (2008).

Data availability

Source data are provided for all experiments. Other data that support the findings of this study are available from the corresponding author, upon reasonable request.

Acknowledgments We thank Masaaki Ozawa, Mai Hasegawa, Takuya Yogi, Mizuki Kanazawa, and Sachi Tsuji for help with the *in vitro* studies, Yuri Sato for help with the *in vivo* studies. We thank the NCI RAS initiative for providing the RAS-less MEFs used in this work, the Uchiro Laboratory for performing the high-resolution mass spectrometry analysis at the Research Equipment Center (Tokyo University of Science (TUS), Japan), the Gunji Laboratory (TUS) for the use of their high-performance liquid chromatography instruments, the Iwakura and Abe Laboratories in the animal facility of the Research Institute for Biomedical Sciences (TUS) for maintaining the mice, Fumito Ishizuka and Naoki Takeda (NARD Institute, Ltd.) for contributions to the chemical synthesis, and Hiroyuki Ohashi for the helpful suggestions. This work was financially

supported by the Program for Creating STart-ups from Advanced Research and Technology (START Program: 962238), and the joint research with FuturedMe Inc.

Author contributions S. Im., L. H., S. It., and E. M. S. designed the study. S. Im., L. H., S. It., M. I., M. T., M. S. and T. Y. performed the *in vitro* and *in vivo* experiments. Y. I. performed chemical analyses. E. M. S. supervised the study. All authors discussed the study and approved the submitted manuscript.

Competing interests The authors declare no competing interests.

Additional Information is available in the online version of the paper.

Figure legends

Fig. 1. RAS chemical knockdown *in vitro*.

a, Principle of the CANDDY technology. Each CANDDY molecule includes a target interactor (burgundy hexagon) and a CANDDY tag (yellow oval). The target protein is bound by the CANDDY molecule *via* the target interactor and is directly degraded by proteasome via the CANDDY tag. **b,** The CANDDY tag was synthesized by chemically inactivating the inhibitor site of MLM2238 (MLN). **c,** Structures of the RAS-SOS inhibitor (ref. 3), RAS-SOS-NH_2, and TUS-007. **d,** Evaluation of the target-binding affinity of TUS-007 to KRAS mutants by a thermal shift assay. Recombinant KRAS was treated with the vehicle, RAS-SOS inhibitor, or TUS-007 for 30 min, heated at the indicated temperature for 20 min, then analyzed by immunoblotting. **e,** KRAS G12D protein level was lower after incubation with TUS-007 at the indicated concentrations in the presence of 26S proteasome, indicating successful KRAS G12D degradation by TUS-007 (mean ± SEM; n = 3). *$P < 0.05$ and ** $P < 0.01$ vs. DMSO. **f,** KRAS G12D and G12V levels, but not the G12C level, were decreased in RAS-less MEFs after

364 incubation with TUS-007 for 72 h. Representative blots are shown. The relative
365 amounts of KRAS mutants normalized to GAPDH are shown in the bar graph (mean ±
366 SEM; n = 3–4). *P < 0.05 and ** P < 0.01 vs. DMSO. **g,** Decreased cell viability was
367 observed in RAS-less MEFs expressing human KRAS G12D and G12V, but not those
368 expressing G12C, after incubation with TUS-007 for 72 h (mean ± SEM; n = 3–4). *P <
369 0.05 and ** P < 0.01 vs. DMSO.
370
371
372 **Fig. 2. Chemical knockdown and tumor suppression *in vitro* and *in vivo* in KRAS**
373 **G12V-driven human colon cancer cells by TUS-007 treatment.**
374 **a,** Immunoblotting analysis of KRAS G12V chemical knockdown in SW620-Luc cells
375 treated with TUS-007 for 48 h at the indicated doses. The KRAS band intensity was
376 normalized to that of GAPDH (mean ± SEM; n = 3). *P < 0.05 and ** P < 0.01 vs.
377 DMSO. **b & c,** TUS-007 induced apoptosis in colon cancer SW620-Luc cells (b) but
378 not in HT29-Luc cells (c), a KRAS-independent, BRAF-dependent cell line (Ctx +
379 Vem: 100 mg/ml cetuximab and 40 μM vemurafenib). Cells were treated with each

compound for 48 h in terms of the number of annexin V-positive/PI-negative apoptotic cells detected by flow cytometry (mean ± SEM; n = 2–5). **P < 0.01, and ***P < 0.001 vs. DMSO. **d,** Relative activity of caspase 3/7 in SW620-Luc cells treated with TUS-007 or 5-fluorouracil (5-FU) for 48 h (mean ± SEM; n = 3). *P < 0.05 and ** P < 0.01 vs. DMSO. **e,** Tumor volume in mice with SW620-Luc cells transplanted subcutaneously and treated with i.p. administration every 3 days (mean ± SEM; n = 6–8). *P < 0.05 vs. vehicle alone. **f,** Immunoblotting of KRAS G12V chemical knockdown in tumors from the same mice used in e (mean ± SEM; n = 6). **P < 0.01 vs. vehicle alone.

Fig. 3. Chemical knockdown and tumor suppression *in vitro* and *in vivo* in KRAS G12D-driven human pancreatic cancer cells by TUS-007 treatment.

a, KRAS G12D chemical knockdown induced by TUS-007 in SW1990 cells. SW1990 cells were treated with TUS-007 for 72 h and analyzed by immunoblotting. The KRAS G12D band intensity was normalized to that of GAPDH (mean ± SEM; n = 4). *P < 0.05 vs. DMSO. **b,** TUS-007 treatment for 72 h increased the proportion of annexin V-

positive apoptotic SW1990 cells compared with those treated with DMSO or RAS-SOS-NH_2 (mean ± SEM; n = 3). *P < 0.05 vs. DMSO or RAS-SOS-NH_2. **c,** TUS-007 increased the caspase 3/7 activity in SW1990 cells after treatment for 96 h (mean ± SEM; n = 3). *P < 0.05 and **P < 0.01 vs. DMSO. **d,** Caspase 3/7 activation by TUS-007 was counteracted by proteasome inhibition by MLN2238 (MLN) but not by E3 ligase inhibition by NAE inhibitor in SW1990 cells treated with the agents for 96 h (mean ± SEM; n = 3). **P < 0.01 vs. DMSO, $^{\#\#}$P < 0.01 vs. TUS-007 (100 μM) only, and †no statistically significant difference compared with TUS-007 (100 μM) only. **e,** Tumor volume in mice with SW1990 cells transplanted subcutaneously and treated with p.o. administered TUS-007 or vehicle (mean ± SEM; n = 6–9). The agents were administered every 3 days. **P < 0.01 vs. vehicle alone. **f,** Body weight changes in mice with SW1990 cells transplanted subcutaneously (mean ± SEM; n = 6–9). P.o. treatment with TUS-007 did not affect the body weight.

Fig. 4. TUS-007 suppresses the growth of KRAS G12D-positive orthotopic pancreatic tumors.

412 **a,** Images showing the luciferase activity and total flux in orthotopic tumors
413 transplanted SW1990-Luc cells *in vivo*. **b,** Tumor growth (bioluminescence) in identical
414 mice treated with vehicle or TUS-007 administered p.o. every 3 days. (mean ± SEM; n
415 = 6). *P < 0.05 vs. vehicle alone. **c,** Representative histochemical staining of KRAS and
416 TUNEL in orthotopic tumor sections from the same mice used in **a.** The scale bar is 60
417 μm. The bar graphs showed quantitative analyses of the KRAS G12D-positive area
418 (left) and TUNEL-positive area (right) (mean ± SEM; n = 6). **P < 0.01 vs. vehicle
419 alone.
420
421 **Supplementary Fig. 1. Estimation of T_m value of KRAS G12D incubated with TUS-**
422 **007.** KRAS G12D was mixed with DMSO, RAS-SOS inhibitor (4 μM) or TUS-007 (4
423 μM) and incubated under heating from 25 °C to 99 °C. The denature of KRAS G12D
424 was monitored by the fluorescence. The typical curve of each group was shown in upper
425 panels. The means of T_m values were shown in lower table (mean ± SEM; n = 2). * P <
426 0.05 vs. DMSO, # P < 0.05 vs. RAS-SOS inhibitor.
427

Supplementary Fig. 2. Effects of TUS-007 on proteasome activity levels.

The levels of chymotrypsin-like (b5), trypsin-like (b2), and caspase-like (b1) proteasome activities was monitored by Suc-LLVY-AMC, Bz-VGR-AMC, and Z-LLE-AMC, respectively. AMC fluorescence was monitored by a plate reader with excitation and emission filters of 360 and 460 nm, respectively (DMSO, 30 min = 1) (mean ± SEM; n = 2-3).

Supplementary Fig. 3. TUS-007 induced degradation of KRAS G12D/V in cell free assay.

a, Evaluation of the correlation between relative amount of KRAS G12D and concentration of TUS-007 were approximated with Rodbard. The DC50 was estimated about 4 μM**. b,** A proteasome inhibitor MLN2238 repressed KRAS G12D chemical knockdown by 26S proteasome. RAS-SOS inhibitor and RAS-SOS NH_2 did not induce KRAS G12D chemical knockdown. KRAS G12D incubated with 26S proteasome and agents as indicated for 3 h. **c,** KRAS G12V protein level was lower after incubation with TUS-007 at the indicated concentrations in the presence of 26S proteasome for 1 h,

444 indicating successful KRAS G12V degradation by TUS-007 (mean ± SEM; n = 3). * P

445 < 0.05 vs. DMSO.

446

447 **Supplementary Fig. 4. Selective chemical knockdown of RAS variants in RAS-less**

448 **MEFs expressing different types of human RAS.**

449 **a,** Relative viability of RAS-less MEFs expressing WT human RAS family members

450 after incubation with TUS-007 or DMSO. (mean ± SEM; n = 3-5). *P < 0.05 and **P <

451 0.01 vs. DMSO. **b,** Degradation of WT human RAS family members in RAS-less MEFs

452 treated with TUS-007 or DMSO for 72 h (mean ± SEM; n = 4-5). *P < 0.05 and **P <

453 0.01 vs. DMSO.

454

455 **Supplementary Fig. 5. FACS plots for Annexin V- PI staining of SW620-Luc cells.**

456 SW620-Luc cells were treated with the indicated agents for 48 h, followed by staining

457 with Annexin V-FITC and PI. The typical plots are shown.

458

459 **Supplementary Fig. 6. FACS plots for Annexin V- PI staining of HT-29-Luc cells.**

460 HT-29-Luc cells were treated with the indicated agents for 48 h, followed by staining

461 with Annexin V-FITC and PI. The typical plots are shown.

462

463 **Supplementary Fig. 7. Effects of TUS-007 on the growth of colon cancer**

464 **subcutaneous xenografts and toxicity.**

465 **a,** Tumors of SW620-Luc cells at day 21 from the same mice shown in Fig. 2e (n = 6–

466 8). **b,** Comparison of SW620-Luc tumor weight at 21 days after injection (mean ± SEM;

467 n = 6–8). *P < 0.05 vs. vehicle alone. **c,** Body weight changes in mice with SW620-Luc

468 cells transplanted subcutaneously (mean ± SEM; n = 6–8). Treatment with TUS-007 did

469 not affect the body weight.

470

471 **Supplementary Fig. 8. Effects of TUS-007 on the growth of pancreatic cancer**

472 **subcutaneous xenografts and toxicity.**

473 **a,** Tumors of SW1990 cells from the same mice shown in Fig. 3e at 21 days after p.o.

474 administration. **b,** Comparison of SW1990 tumor weight in a in this figure at 21 days

475 after p.o. administration (mean ± SEM; n = 6-9). *P < 0.05 vs. vehicle alone. **c,** Tumor

476 volume in mice with SW1990 cells transplanted subcutaneously and treated with i.p.
477 administered TUS-007 or vehicle (mean ± SEM; n = 6-9). The agents were
478 administered every three days. *P < 0.05 vs. vehicle. **d,** Body weight changes in mice
479 with SW1990 cells transplanted subcutaneously (mean ± SEM; n = 6-9). i.p. treatment
480 with TUS-007 did not affect the body weight.
481
482 **Supplementary Fig. 9. Effect of TUS-007 on RAS signaling in of pancreatic cancer**
483 **subcutaneous xenografts.**
484 Immunoblotting of KRAS and downstream signaling molecules in tumors from the
485 same mice used in Fig 3a (**a**: p.o treatment) and Supplementary Fig.8c (**b**: i.p.
486 treatment). The quantitative analysis of the immunoblotting was shown as bar graph,
487 where the KRAS values were normalized to GAPDH, the p-ERK values were
488 normalized to the total ERK, and the p-AKT values were normalized to the total AKT
489 (mean ± SEM; n = 6). *P < 0.05 vs. vehicle.
490

Supplementary Fig. 10. Effects of oral treatment with TUS-007 on wild type RAS in pancreas.

The immunoblotting analyses of wt RAS proteins in pancreas from the same mice shown in Fig. 3e. TUS-007 degraded KRAS and HRAS but not NRAS (mean ± SEM; n = 6-9). *P < 0.05 vs. vehicle alone.

Supplementary Fig. 11. Effect of TUS-007 on growth of orthotopic pancreatic cancer xenografts expressing mutant KRAS.

a, Tumor growth, as assessed by luciferase signal, in individual mice orthotopically transplanted SW1990-Luc cells treated with TUS-007 (red) or vehicle alone (blue) (mean ± SEM; n = 6). **b,** Pancreases from orthotopic xenograft model mice at day 21 after treatment with TUS-007 (lower-left panel) or the vehicle alone (upper-left panel) and comparison of their weights (right graph) (mean ± SEM; n = 6). *P < 0.05 vs. vehicle alone. **c,** Immunoblotting of KRAS G12D in tumor lysates from the same mice used in Fig. 4a. The bar graph shows quantification of KRAS G12D normalized to GAPDH (mean ± SEM; n = 6). **P < 0.01 vs. vehicle alone. **d,** Body weight changes in

mice subjected to orthotopical transplantation of SW1990-Luc cells (mean ± SEM; n = 6). Treatment with TUS-007 did not affect the body weight.

Supplementary Fig. 12. CANDDY induced degradation of MDM2, a common undruggable target.

a, The structure of MDM2-CANDDY using P53-MDM2 PPI inhibitor, with IC50 value between 6-25 μM. **b,** The human colon cancer cells HCT-116 were incubated for 48 h with MDM2-CANDDY. MDM2-CANDDY degraded MDM2 in the dose dependent manner (mean ± SEM. n = 3). ** $P < 0.01$ vs. DMSO.

Methods

Cell lines. SW1990 and HCT-116 cells were purchased from the American Type Culture Collection (Manassas, VA, USA). SW620-Luc and HT29-Luc cells were purchased from the National Institute of Biomedical Innovation, Health, and Nutrition

(Osaka, Japan). RAS-less MEF cell lines (wild-type (wt) KRAS, KRAS G12D, KRAS G12V, KRAS G12C, NRAS and HRAS) were obtained from the National Institutes of Health (NCI RAS Initiative at the Frederick National Laboratory for Cancer Research, Frederick, MD, USA).

Animal studies. BALB/cA-nu/nu and BALB/cA (female, 7-9 weeks old) were purchased from CLEA Japan (Tokyo, Japan). The animals were maintained in conventional housing conditions, with a daily 12-h light/dark cycle, and given food and water *ad libitum*. The animals were cared for in accordance with the NIH Guide for the Care and Use of Laboratory Animals. All animal experiments were approved by the Committee on Animal Experimentation of the Tokyo University of Science.

Reagents. MLN2238 (A10600) was purchased from AdooQ BioScience (Irvine, CA, USA). NAEi was purchased from AdipoGen (San Diego, CA, USA). Human 26S Proteasome Protein (E-365) and Human 20S Proteasome Protein (E-360) were purchased from R&D Systems (Minneapolis, MN, USA). Human KRAS (G12D) and

539 the corresponding His tag (12259-H07E1) were purchased from Sino Biological
540 (Beijing, China). Human KRAS (G12V), 2-186, and the corresponding His tag (R06-
541 32BH) were obtained from SignalChem Lifesciences (Richmond, British Columbia,
542 Canada).
543
544 **Measurement of 20S proteasome activity.** The chymotrypsin-like (β5), trypsin-like
545 (β2), and caspase-like (β1) activities of the 20S proteasome were measured using a 20S
546 Proteasome Activity Kit GOLD (StressMarq Bioscience Inc., Victoria, British
547 Columbia, Canada). Purified 20S proteasome (0.1 μg) was incubated in the presence of
548 CANDDY molecules (1, 4, 10, 20, 40, 80, and 160 μM) or MLN2238 at the indicated
549 concentrations for 30 min at room temperature. After incubation, 100 mM of
550 fluorogenic peptide substrates, Suc-LLVY-AMC (β5 substrate), Bz-VGR-AMC (β2
551 substrate), or Z-LLE-AMC (β1 substrate), was added, followed by incubation for 1 h at
552 room temperature. The reaction mixture was then transferred to a 96-well plate, and the
553 fluorecence from hydrolyzed AMC groups was measured using a Synergy HT multi-

554 channel microplate reader (BioTek Instruments, Inc., Winooski, VT, USA) with a 360
555 nm excitation filter and 460 nm emission filter.
556
557 **Evaluation of affinity of TUS-007 for KRAS in a thermal shift assay.** The KRAS
558 G12D/V (100 nM) was preincubated with TUS-007, a RAS-SOS inhibitor, or 10%
559 DMSO in 75 mM phosphate buffer (pH 7.5) for 30 min at 37 °C (G12D) or for 20 min
560 at 25 °C (G12V). Aliquots of the reaction solution were sampled into separate
561 microtubes and heated for 30 min at 70, 80, or 90 °C for G12D, or at 40, 50, or 60 °C
562 for G12V. After centrifugation at 18,000 ×*g* for 20 min, the supernatants were analyzed
563 by SDS-PAGE, followed by immunoblotting using an anti-KRAS antibody (1:1000,
564 WH0003845MI, Sigma-Aldrich, St. Louis, MO, USA). Immunoreactive bands were
565 detected using an iBright CL1000 chemiluminator (Thermo Fisher Scientific, Waltham,
566 MA, USA) with an enhanced chemiluminescent substrate for detection of horseradish
567 peroxidase (HRP; Merck, Darmstadt, Germany).
568

569 **Estiamtion of T_m values using fluorescence based thermal shift assay.** To estimate
570 the T_m values, we performed a fluorescence based thermal shift assay using ProteoStat
571 Thermal Shift Stability assay (ENZO Life Sciences, Farmingdale, NY, USA). 1 μg of
572 KRAS G12D was mixed with DMSO (2.5 %), RAS-SOS inhibitor (4 μM) or TUS-007
573 (4 μM) in 1x assay buffer containing a fluorescent indicator of protein destabilization,
574 ProteoStat TS Detection Reagent, and incubated under heating from 25 °C to 99 °C in
575 StepOne Plus Real-time PCR system (Thermo Fisher Scientific). The kinetics of
576 fluorescent signals were analyzed to calculate T_m values in Protein Thermal Shift
577 Software 1.3 (Thermo Fisher Scientific).
578
579 **Evaluation of KRAS degradation induced by TUS-007 in a cell-free system.** KRAS
580 G12D (final concentration: 5 ng/μL) and 26S proteasome (final concentration: 8 nM)
581 were incubated with TUS-007 (2, 3, 5, 10, 20, 40 μM), RAS-SOS inhibitor (40 μM),
582 RAS-SOS-NH_2 (40 μM) or DMSO in 20 mM Tris-HCl buffer (pH 7.5) containing 20%
583 glycerol for 3 h at 37 °C. To assess the effect of MLN on chemical knockdown, KRAS
584 G12D and 26S proteasome were incubated with DMSO or TUS-007 40 μM in the

presence or absence of MLN (1 μM) in the same condition. KRAS G12V (final concentration: 5 ng/μL) and 26S proteasome (final concentration: 8 nM) were incubated with TUS-007 at the indicated concentration or DMSO in 75 mM phosphate buffer, containing 1% LABRASOL (Gattefossé, Saint-Priest, France), for 1 h at 37 °C. After centrifugation at 14,000 ×*g* for 10 min, the supernatants were analyzed by SDS-PAGE, followed by immunoblotting using an anti-KRAS antibody (1:1000, WH0003845MI for G12D, Sigma-Aldrich; and 1:2000, F234 for G12V, Santa Cruz Biotechnology, Inc., Dallas, TX, USA). The immunoreactive bands were detected, as described above. The DC_{50} values were calculated by a Rodbard approximation using the band intensity obtained from four and three independent experiments for G12D. Immunoblotting was performed as mentioned above.

Cell proliferation assay. To examine the effect of TUS-007 on cell proliferation, the WST-8 assay (Cell Count Reagent SF; Nacalai Tesque, Kyoto, Japan) was performed. RAS-less MEF cells, expressing human RAS, were plated in 96-well plates at a density of 3×10^3 cells per well, cultured overnight, then treated with the indicated

601 concentrations of TUS-007 in 4% FBS containing medium (KRAS G12D), 10% FBS
602 containing medium (KRAS G12V) or serum-free medium (KRAS G12C, wt KRAS,
603 HRAS, NRAS) for 72 h. After incubation, cell viability was measured
604 spectrophotometrically using the WST-8 reagent. The culture medium was removed and
605 WST-8 reagent was mixed with the growth medium at a ratio of 1:10 (with a final
606 volume of 110 μL) and added to each well. The cells were incubated in an atmosphere
607 of 5% CO_2 at 37 °C for 1 to 2 h, and the absorbance at 450 nm was measured using the
608 aforementioned Synergy HT multi-channel microplate reader (BioTek Instruments,
609 Inc.).
610
611 **Evaluation of TUS-007 specificity in cells.** RAS-less MEFs were used to evaluate the
612 selective degradation by TUS-007. RAS-less MEFs expressing one of the human WT
613 RAS members (KRAS WT, HRAS WT, or NRAS WT) or KRAS G12C were plated
614 into 6-well plates at a density of 3×10^4 cells per well, cultured overnight, and treated
615 with the indicated concentrations of TUS-007 in serum-free medium for 72 h. RAS-less
616 MEFs expressing KRAS G12D or G12V were plated into 96-well plates at a density of

617 3×10^3 cells per well, cultured overnight, and treated with the indicated concentrations
618 of TUS-007 in 4% FBS or 10% FBS containing medium, respectively, for 72 h. The
619 cells were lysed using RIPA buffer (Nacalai Tesque., Kyoto, Japan). The lysates were
620 centrifuged at 18,000 ×*g* for 10 min. The supernatants were analyzed by western
621 blotting using mouse monoclonal antibodies specific to KRAS (1:1000,
622 WH0003845MI; Sigma-Aldrich) and glyceraldehyde 3-phosphate dehydrogenase
623 (GAPDH, 1:10000, sc-32233; Santa Cruz Biotechnology, Inc.) and rabbit polyclonal
624 antibodies specific for HRAS (1:1000, 18295-1-AP; Proteintech, Rosemont, IL, USA)
625 and NRAS (1:1000, 10724-1-AP, Proteintech). Immunoreactive bands were detected
626 using iBright CL1000 chemiluminator or LAS 3000 (Fujifilm, Tokyo, Japan) with an
627 enhanced chemiluminescent substrate for the detection of horseradish peroxidase (HRP;
628 Merck, Darmstadt, Germany). The intensity of the RAS band was quantified using
629 ImageJ software and normalized to the intensity of the GAPDH band.
630
631 **Measurement of KRAS protein levels in cells by western blotting.** SW620-Luc and
632 SW1990 cells were treated with 1% DMSO or TUS-007 in serum-free medium for 48 h

633 (SW620-Luc cells) or 72 h (SW1990 cells). The cells were lysed using a RIPA buffer
634 (Nacalai Tesque., Kyoto, Japan). The precipitates were separated from the soluble
635 fraction by centrifugation at 18,000 ×*g* for 20 min. The supernatants were analyzed by
636 western blotting with mouse monoclonal antibodies specific for KRAS (1:1000,
637 WH0003845MI; Sigma-Aldrich) and GAPDH (1:20000, sc-32233; Santa Cruz
638 Biotechnology, Inc.). The immunoreactive bands were detected by LAS-3000, as
639 described above. The intensity of the KRAS band was quantified using ImageJ software
640 and normalized to the intensity of the GAPDH band.
641
642 **Evaluation of caspase activity.** To measure caspase activity, SW1990 cells were plated
643 onto 96-well white plates and 96-well clear plates, at a concentration of 8×10^3
644 cells/well, in a medium containing 10% FBS. The plates were incubated overnight
645 without CO_2 equilibration at 37 °C. The medium was replaced with medium containing
646 2% FBS, DMSO, 100 μM TUS-007, 3 μM MLN2238, or 2.5 μM NAEi and incubated
647 for 96 h. SW620-Luc cells were plated onto 96-well white plates and 96-well clear
648 plates at 2×10^3 cells/well in medium containing 10% FBS. After overnight incubation,

649 the medium was replaced with FBS-free medium containing 1% L-glutamine, DMSO,
650 and 25, 100, or 500 μM TUS-007 for 48 h. The caspase 3/7 Glo assay (Promega,
651 Madison, WI, USA) was performed on the white plates according to the manufacturer's
652 protocol. The chemiluminescence intensity was measured with a Synergy HT plate
653 reader (BioTek). The cell viability was measured in the clear plates using the WST-8
654 assay, as described above. Caspase 3/7 activity was obtained as the chemical
655 luminescence intensity of the caspase 3/7 Glo assay normalized to the cell viability.
656
657 **Analysis of apoptosis by flow cytometry.** SW1990, SW620-Luc, and HT-29 cells
658 were seeded in 24-well plates, followed by the addition of compounds at the indicated
659 concentrations. After incubation for 48 h (SW620-Luc, HT-29) or 72 h (SW1990), the
660 cells were harvested using trypsin, washed with phosphate-buffered saline (PBS), and
661 pelleted by centrifugation at 110 ×g for 5 min. The cells were resuspended in 85 μL of
662 binding buffer (Annexin V-FITC Kit, Medical & Biological Laboratories Co., Ltd.,
663 Nagoya, Japan). Subsequently, 10 μL of annexin V-FITC and 5 μL of propidium iodide
664 (PI) were added to each sample, followed by incubation in the dark at room temperature

665 for 15 min. After incubation, 400 μL of binding buffer was added to each sample on ice.
666 The cells were then analyzed using a FACSCanto II fluorescence-activated cell sorter
667 (BD Biosciences, Santa Clara, CA, USA) to detect the fluorescein isothiocyanate
668 (FITC) signal with excitation and emission filter wavelengths of 488 nm and 580 nm,
669 respectively, to detect the PI signal. Data were analyzed using FlowJo software
670 (FlowJo, Eugene, OR, USA).
671
672 **Subcutaneous xenograft model.** SW620-Luc (3×10^7 cells/mL) and SW1990 (5×10^7
673 cells/mL) cells were suspended in PBS, and 100 μL of the single-cell suspension was
674 transplanted subcutaneously into the right flanks of BALB/cA-nu/nu mice using a 26 G
675 syringe. Tumor volumes were calculated as the tumor length $\times$ width$^2 \times 0.5$. When the
676 tumor volumes reached approximately 100 mm^3, the mice were randomized into
677 treatment and control groups of 6 to 8 animals per group. For i.p. treatment, TUS-007
678 was dissolved in DMSO and then diluted to a final concentration of 10% DMSO in 20%
679 polyethylene glycol (PEG) 400/Tween 80 (1:1 ratio). The TUS-007 solution was
680 administered intraperitoneally into the tumor-bearing mice at a dose of 80 mg/kg every

three days. The control mice were treated with the PEG/Tween vehicle alone. For p.o. treatment, TUS-007 was suspended in 0.5% (w/v) carboxymethyl cellulose (CMC) and administered p.o. at a dose of 80 mg/kg every three days. CMC (0.5% w/v) was administered to control mice. Cetuximab was administered to an additional group of SW620-Luc-implanted mice at a dose of 1 mg/mouse every three days.

Orthotopic xenograft model. The pGL4.51 (Luc2/CMV/Neo) vector (Promega) was transfected into SW1990 cells. Successfully transfected cells were selected using G418. SW1990-Luc cells were mixed with growth factor-reduced Matrigel (BD Biosciences) on ice, at a ratio of 1:1 (v/v), to obtain a final cell density of 1.5×10^4 cells/μL. Ten microliters of the cell suspension was injected directly into the pancreas of BALB/cA-nu/nu mice using a 27 G syringe. Three days after cell transplantation, TUS-007 treatment was initiated in six mice. TUS-007 was suspended in 0.5% (w/v) CMC and administered orally at a dose of 160 mg/kg every 3 days. CMC (0.5% w/v) was administered to control mice (n = 6). Tumor luciferase activity was monitored based on the bioluminescence intensity. Fifty microliters of D-luciferin (30 mg/mL in saline) was

697 injected subcutaneously in mice (Promega). Twenty minutes after the injection,
698 bioluminescence images were obtained using an IVIS Lumina LT (Perkin Elmer,
699 Waltham, MA, USA) with an exposure time of 15 s while the mice were under
700 isoflurane anesthesia (Wako, Tokyo, Japan).
701
702 **Measurement of RAS levels and downstream signaling molecule activation in**
703 **xenograft tumors.** KRAS expression in xenograft tumors and wt RAS protein
704 expression in pancreas were evaluated by immunohistochemistry and western blot
705 analysis. Tumor tissue and pancreas were harvested from the mice harboring
706 subcutaneous xenografts on day 21 of the TUS-007 administration. Tumor tissues were
707 harvested from the orthotopic xenograft mice on day 24 after the TUS-007
708 administration for consecutive 3 days starting on day 21. A portion of each sample was
709 fixed in 4% paraformaldehyde (Nacalai Tesque., Kyoto, Japan), embedded in paraffin,
710 then cut into 5 μm-thick sections. The sections were deparaffinized and incubated in
711 0.3% hydrogen peroxide in methanol for 30 min, and antigen retrieval was performed
712 using a 10 mM citrate buffer (pH 6.0) at 121 °C for 20 min. Tumor tissues were

713 subsequently blocked with 1% bovine serum albumin (BSA) in PBS for 30 min and
714 stained with primary antibodies specific for human KRAS (1:200, 12063-1-AP;
715 Proteintech), diluted in 1% BSA, followed by HRP-labeled secondary antibodies
716 (1:600, ab6721; Abcam, Cambridge, UK) in 1% BSA for 30 min at room temperature.
717 The sections were counterstained with hematoxylin and visualized with
718 diaminobenzidine (1.02924.0001; Merck). Digital images were obtained at 40×
719 magnification using a model BZ-9000 microscope (Keyence, Osaka, Japan). The area of
720 KRAS staining was quantified using ImageJ software, and the perimeter-to-area ratio
721 (KRAS-positive area/section) was calculated for a total of 30 images of 6 tumor
722 sections from each group. The remaining part of each tumor sample was homogenized
723 in a cell-lysis buffer (50 mM triethanolamine, 50 mM KCl, 5 mM $MgCl_2$, 0.25 M
724 sucrose, 1 mM phenylmethylsulfonyl fluoride, proteinase inhibitors (Nacalai Tesque.,
725 Kyoto, Japan), 1 mM dithiothreitol, and ribonuclease inhibitor (0.2 unit/μl, TaKaRa
726 Bio., Shiga, Japan) for western blot analysis, as described above. Mouse monoclonal
727 antibodies specific for KRAS (1:1000, WH0003845MI; Sigma-Aldrich), HRAS
728 (1:1000, 18295-1-AP; Proteintech, Rosemont, IL, USA), NRAS (1:1000, 10724-1-AP,

729 Proteintech) and GAPDH (1:20000, sc-32233; Santa Cruz Biotechnology, Inc.) and
730 rabbit antibodies specific for p-Erk1/2 (phospho-p44/42 MAPK) (1:1000, #4370; Cell
731 Signaling Technology, Beverly, MA, USA), Erk1/2 (p44/42 MAPK) (1:1000, #4695;
732 Cell Signaling Technology), p-Akt (1:2000, #4060; Cell Signaling Technology), and
733 Akt (1:2000; #4691; Cell Signaling Technology) were used for the
734 immunohistochemical staining. The immunoreactive bands were detected by LAS-3000
735 as described above. Quantitative analysis of the western blots was performed using
736 ImageJ software, and the results were normalized to the GAPDH band intensity.
737
738 **Measurement of apoptosis in xenograft tumors.** DNA fragmentation in the tumor
739 tissues was evaluated by a TdT-mediated dUTP nick-end labeling (TUNEL) assay.
740 Paraffin-embedded tissue sections (5 μm thick) were deparaffinized. The TUNEL
741 reaction was performed using the DeadEnd Fluorometric TUNEL System (Promega),
742 according to the manufacturer's instructions. Fluorescence images were acquired using a
743 BZ-9000 fluorescence microscope (Keyence). TUNEL-positive cells were identified

744 and counted using ImageJ software. In total, 30 images of 6 tumor sections were
745 analyzed from each group.
746
747 **Determination of TUS-007 in pancreas.** BALB/c mice were treated i.p. with TUS-007,
748 and pancreas tissue was collected at suitable time points. Approximately 30-60 mg of
749 tissue was homogenized in 0.6 mL of tissue-lysis buffer (50 mM Tris-HCl pH 8.0, 20
750 mM EDTA, 10 mM NaCl, 1% SDS) by Micro Smash MS-100 using stainless (5.5 ϕ) and
751 zirconia (1.0 ϕ) beads (TOMY SEIKO CO., LTD., Tokyo, Japan), and 1 μL propyl p-
752 hydroxybenzoate (4 mg/mL in DMSO) was added to each sample as an internal standard.
753 Lysates were centrifuged at 18,000 ×*g* for 10 min and 2.25 mL of methanol/chloroform
754 (ratio of 2:1) was added to the supernatants and the mixture was allowed to stand for 30
755 min at room temperature. Chloroform and distilled water (0.75 mL each) were added and
756 samples were centrifuged at 1,500 ×*g* for 15 min. The layer of chloroform was collected.
757 The supernatants were dried under reduced pressure and redissolved in the mobile phase.
758 TUS-007 was determined by HPLC (Alliance e2695, Waters Corporation., MA, USA)
759 using COSMOSIL® C18-AR-II column (150×4.6 mm, Nacalai Tesque., Kyoto, Japan) in

760 the isocratic elution mode with 0.1% trifluoroacetic acid (TFA) in 50:50 (v/v)
761 acetonitrile/water mobile phase at a flow rate of 1.0 mL/min. All reagents for the assay
762 were purchased from Nacalai Tesque. (Kyoto, Japan).
763
764 **Degradation of MDM2 in HCT-116 cells.** HCT-116 human colon-cancer cells were
765 treated with 1% DMSO or TUS-007 in serum-free medium for 24 h. The cells were
766 lysed using a RIPA buffer (Nacalai Tesque). The precipitates were separated from the
767 soluble fraction by centrifugation at 18,000 ×*g* for 20 min. The supernatants were
768 analyzed by western blotting using a rabbit polyclonal antibody specific for MDM2
769 (1:1000, sc-965, Santa Cruz Biotechnology, Inc.) and GAPDH (1:20000, sc-32233;
770 Santa Cruz Biotechnology, Inc.). The immunoreactive bands were detected by LAS-
771 3000, as described above. The intensity of the MDM2 band was quantified using
772 ImageJ software and normalized to the intensity of the GAPDH band.
773
774 **Statistical analyses.** Statistical significance was determined with JMP® Pro 14 (SAS
775 Institute Inc., Cary, NC, USA). An unpaired *t*-test was used to compare pairs of groups

776 under the assumption of normality. A one-way ANOVA with Dunnett's post hoc

777 analysis was used to compare sets of three or more groups. P-values < 0.05 were

778 considered statistically significant.

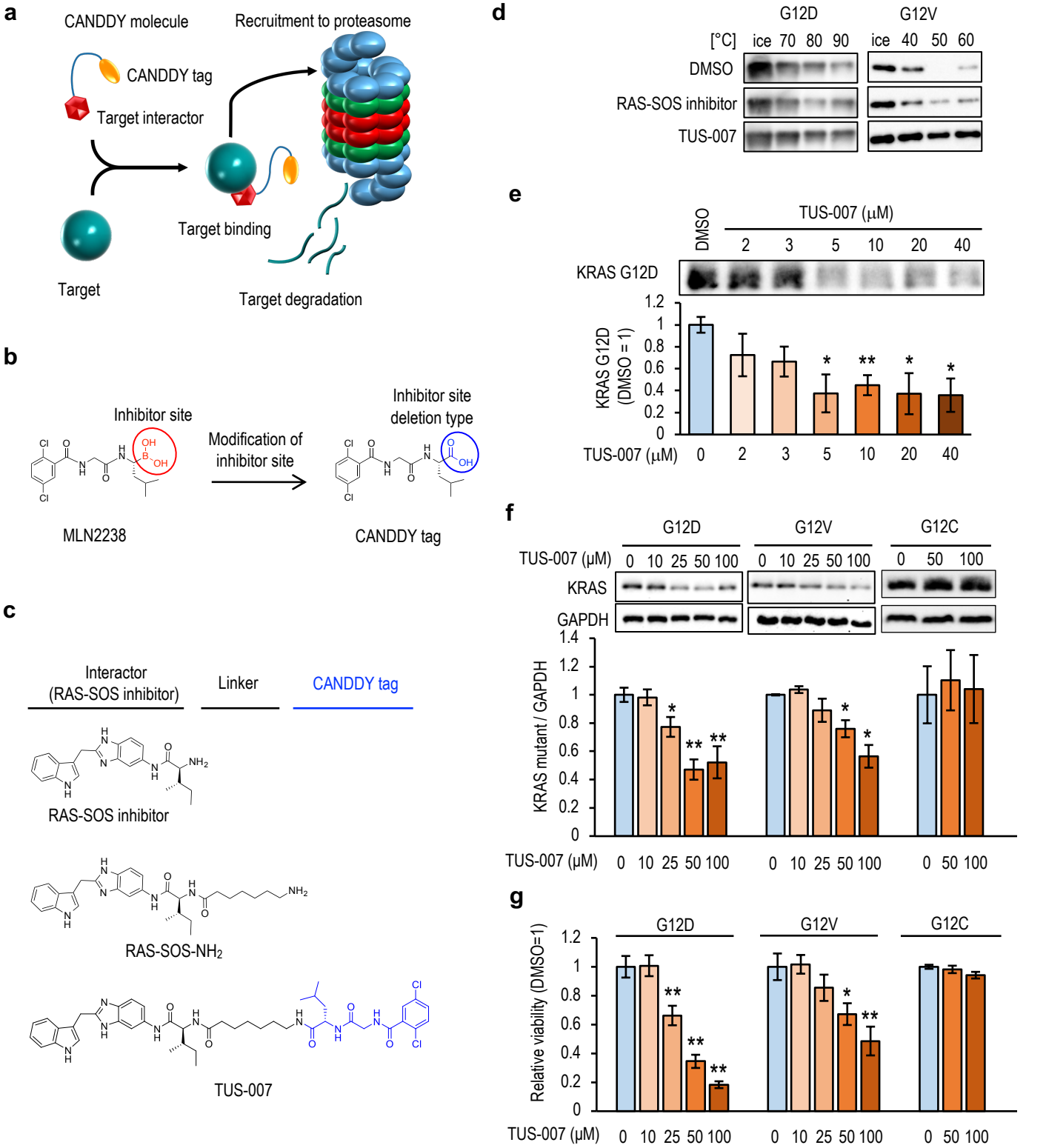

Fig. 1. RAS chemical knockdown *in vitro*.

a, Principle of the CANDDY technology. Each CANDDY molecule includes a target interactor (burgundy hexagon) and a CANDDY tag (yellow oval). The target protein is bound by the CANDDY molecule *via* the target interactor and is directly degraded by proteasome via the CANDDY tag. **b,** The CANDDY tag was synthesized by chemically inactivating the inhibitor site of MLM2238 (MLN). **c,** Structures of the RAS-SOS inhibitor (ref. 3), RAS-SOS-NH_2, and TUS-007. **d,** Evaluation of the target-binding affinity of TUS-007 to KRAS mutants by a thermal shift assay. Recombinant KRAS was treated with the vehicle, RAS-SOS inhibitor, or TUS-007 for 30 min, heated at the indicated temperature for 20 min, then analyzed by immunoblotting. **e,** KRAS G12D protein level was lower after incubation with TUS-007 at the indicated concentrations in the presence of 26S proteasome, indicating successful KRAS G12D degradation by TUS-007 (mean ± SEM; n = 3) . *P < 0.05 and ** P < 0.01 vs. DMSO. **f,** KRAS G12D and G12V levels, but not the G12C level, were decreased in RAS-less MEFs after incubation with TUS-007 for 72 h. Representative blots are shown. The relative amounts of KRAS mutants normalized to GAPDH are shown in the bar graph (mean ± SEM; n = 3–4). *P < 0.05 and ** P < 0.01 vs. DMSO. **g,** Decreased cell viability was observed in RAS-less MEFs expressing human KRAS G12D and G12V, but not those expressing G12C, after incubation with TUS-007 for 72 h (mean ± SEM; n = 3–4). *P < 0.05 and ** P < 0.01 vs. DMSO.

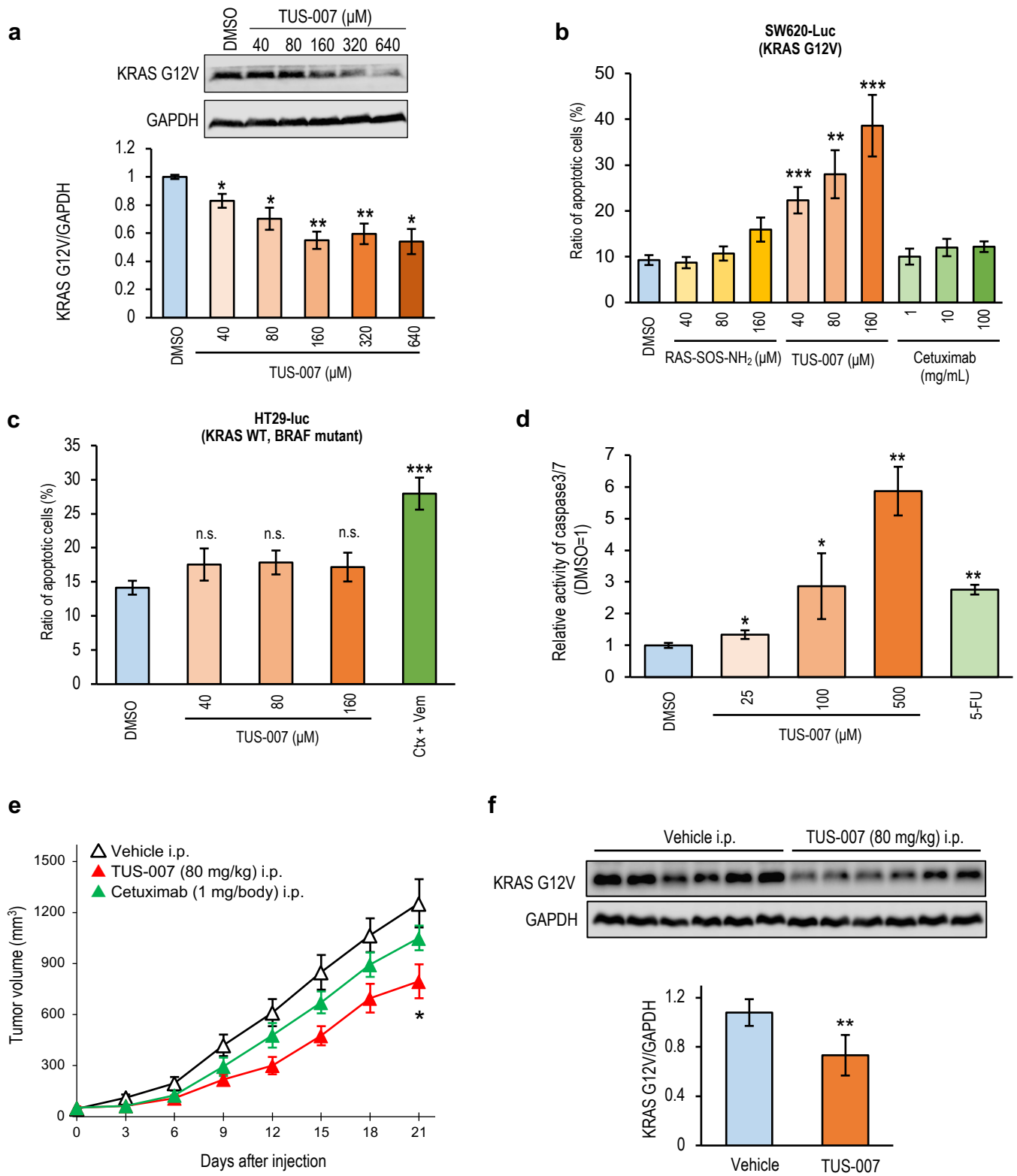

Fig. 2. Chemical knockdown and tumor suppression *in vitro* and *in vivo* in KRAS G12V-driven human colon cancer cells by TUS-007 treatment.

a, Immunoblotting analysis of KRAS G12V chemical knockdown in SW620-Luc cells treated with TUS-007 for 48 h at the indicated doses. The KRAS band intensity was normalized to that of GAPDH (mean ± SEM; n = 3). *P < 0.05 and ** P < 0.01 vs. DMSO. **b & c,** TUS-007 induced apoptosis in colon cancer SW620-Luc cells (**b**) but not in HT29-Luc cells (**c**), a KRAS-independent, BRAF-dependent cell line (Ctx + Vem: 100 μg/ml cetuximab and 40 μM vemurafenib). Cells were treated with each compound for 48 h in terms of the number of annexin V-positive/PI-negative apoptotic cells detected by flow cytometry (mean ± SEM; n = 2–5). **P < 0.01, and ***P < 0.001 vs. DMSO. **d,** Relative activity of caspase 3/7 in SW620-Luc cells treated with TUS-007 or 5-fluorouracil (5-FU) for 48 h (mean ± SEM; n = 3). *P < 0.05 and ** P < 0.01 vs. DMSO. **e,** Tumor volume in mice with SW620-Luc cells transplanted subcutaneously and treated with i.p. administration every 3 days (mean ± SEM; n = 6–8). *P < 0.05 vs. vehicle alone. **f,** Immunoblotting of KRAS G12V chemical knockdown in tumors from the same mice used in **e** (mean ± SEM; n = 6). **P < 0.01 vs. vehicle alone.

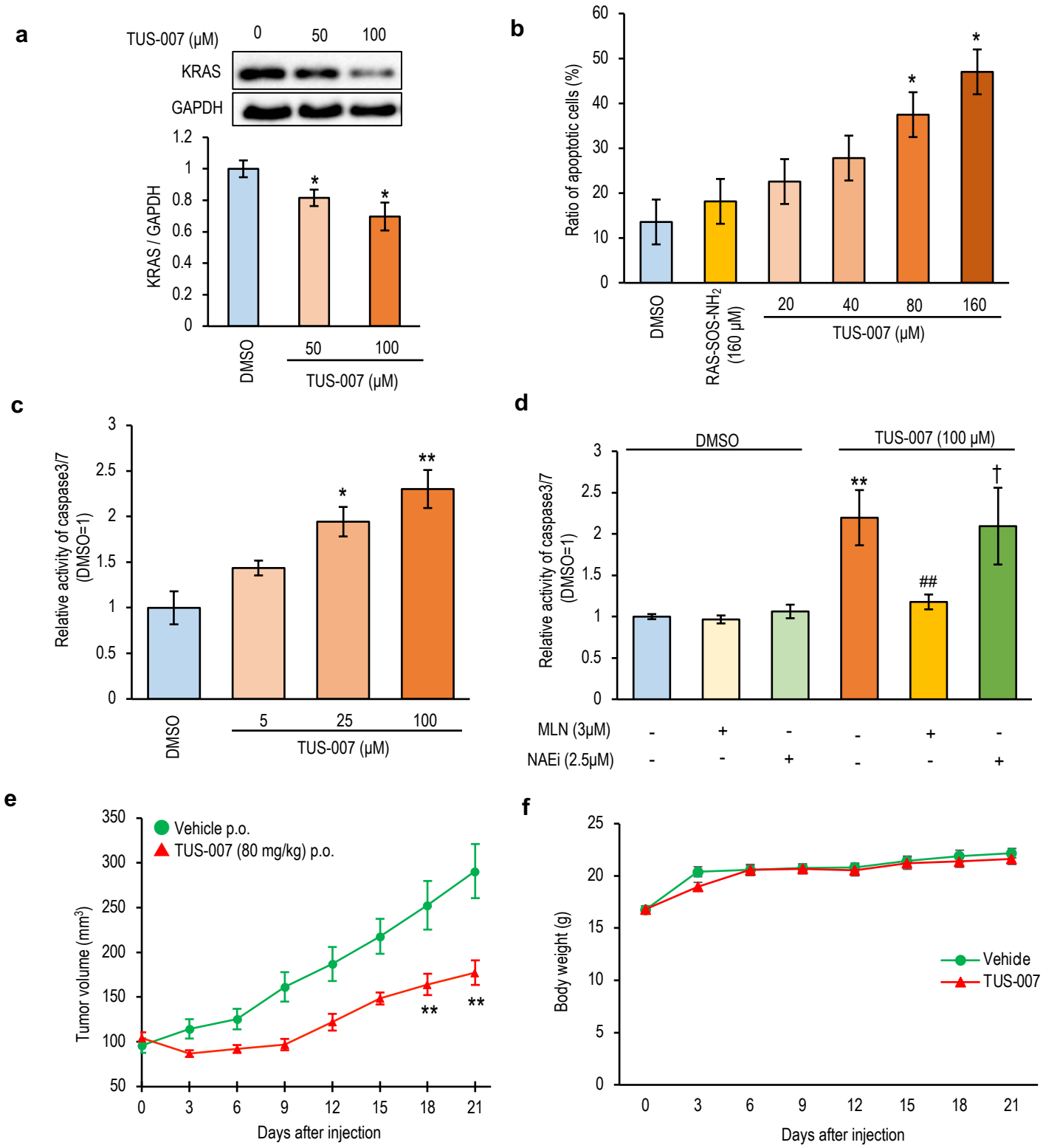

Fig. 3. Chemical-knockdown and tumor suppression *in vitro* and *in vivo* in KRAS G12D-driven human pancreatic cancer cells by TUS-007 treatment.

a, KRAS G12D chemical knockdown induced by TUS-007 in SW1990 cells. SW1990 cells were treated with TUS-007 for 72 h and analyzed by immunoblotting. The KRAS G12D band intensity was normalized to that of GAPDH (mean ± SEM; n = 4). *P < 0.05 vs. DMSO. **b,** TUS-007 treatment for 72 h increased the proportion of annexin V-positive apoptotic SW1990 cells compared with those treated with DMSO or RAS-SOS-NH_2 (mean ± SEM; n = 3). *P < 0.05 vs. DMSO or RAS-SOS-NH_2. **c,** TUS-007 increased the caspase 3/7 activity in SW1990 cells after treatment for 96 h (mean ± SEM; n = 3). *P < 0.05 and **P < 0.01 vs. DMSO. **d,** Caspase 3/7 activation by TUS-007 was counteracted by proteasome inhibition by MLN2238 (MLN) but not by E3 ligase inhibition by NAE inhibitor in SW1990 cells treated with the agents for 96 h (mean ± SEM; n = 3). **P < 0.01 vs. DMSO, ##P < 0.01 vs. TUS-007 (100 μM) only, and †no statistically significant difference compared with TUS-007 (100 μM) only. **e,** Tumor volume in mice with SW1990 cells transplanted subcutaneously and treated with p.o. administered TUS-007 or vehicle (mean ± SEM; n = 6–9). The agents were administered every 3 days. **P < 0.01 vs. vehicle alone. **f,** Body weight changes in mice with SW1990 cells transplanted subcutaneously (mean ± SEM; n = 6–9). P.o. treatment with TUS-007 did not affect the body weight.

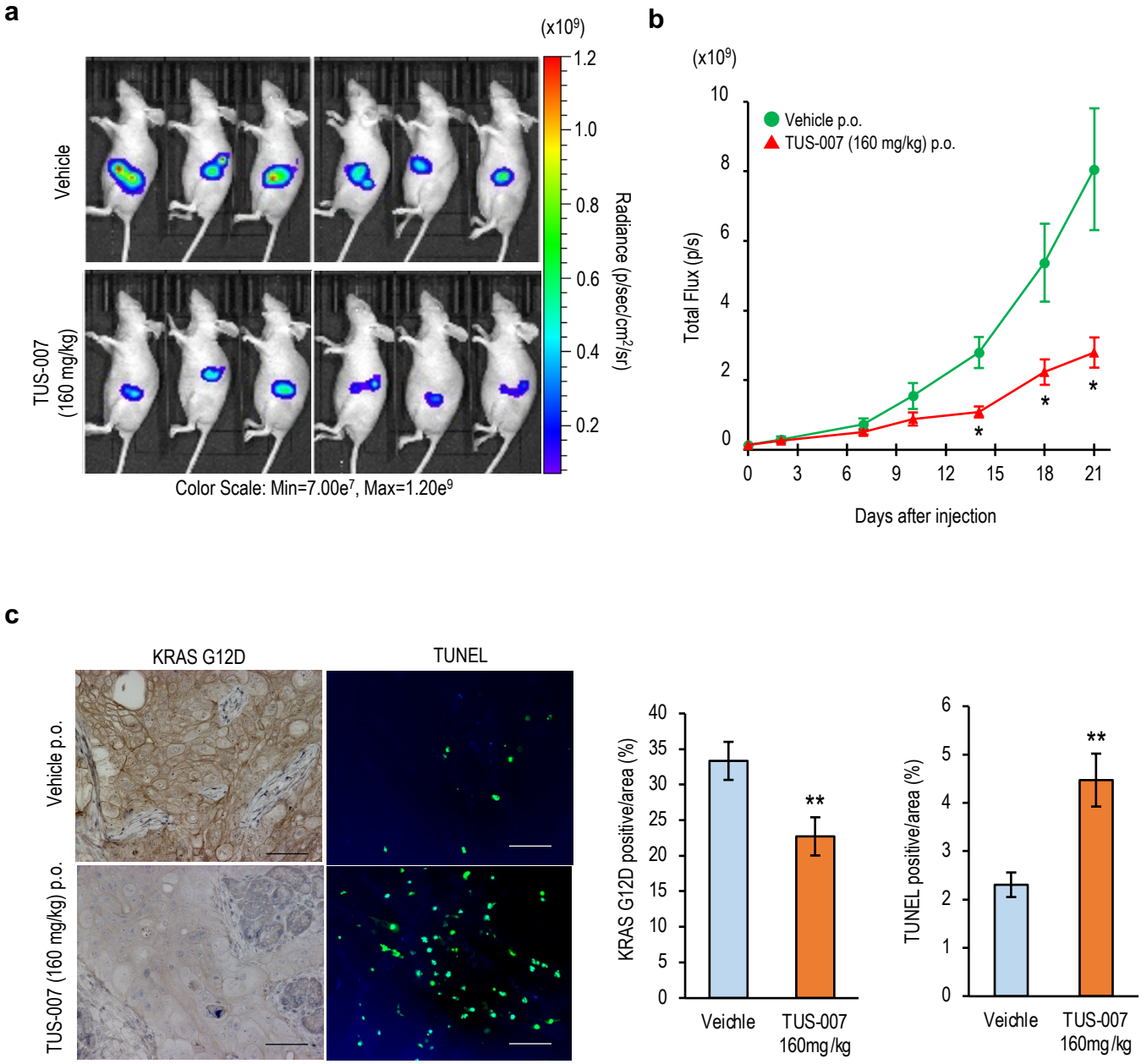

Fig. 4. TUS-007 suppresses the growth of KRAS G12D-positive orthotopic pancreatic tumors.
a, Images showing the luciferase activity and total flux in orthotopic tumors transplanted SW1990-Luc cells *in vivo*. **b,** Tumor growth (bioluminescence) in identical mice treated with vehicle or TUS-007 administered p.o. every 3 days. (mean ± SEM; n = 6). *P < 0.05 vs. vehicle alone. **c,** Representative histochemical staining of KRAS and TUNEL in orthotopic tumor sections from the same mice used in **a**. The scale bar is 60 μm. The bar graphs showed quantitative analyses of the KRAS G12D-positive area (left) and TUNEL-positive area (right) (mean ± SEM; n = 6). **P < 0.01 vs. vehicle alone.